

# Lipid-coated iron oxide nanoparticles for dual-modal imaging of hepatocellular carcinoma

Jinying Liang<sup>1-3</sup>  
Xinxin Zhang<sup>2</sup>  
Yunqiu Miao<sup>2</sup>  
Juan Li<sup>1</sup>  
Yong Gan<sup>2</sup>

<sup>1</sup>Department of Pharmaceutics, China Pharmaceutical University, Nanjing, People's Republic of China; <sup>2</sup>Shanghai Institute of Materia Medica, Chinese Academy of Sciences, Shanghai, People's Republic of China; <sup>3</sup>School of Pharmacy, Xinxiang Medical University, Xinxiang, People's Republic of China

**Abstract:** The development of noninvasive imaging techniques for the accurate diagnosis of progressive hepatocellular carcinoma (HCC) is of great clinical significance and has always been desired. Herein, a hepatocellular carcinoma cell-targeting fluorescent magnetic nanoparticle (NP) was obtained by conjugating near-infrared fluorescence to the surface of Fe<sub>3</sub>O<sub>4</sub> (NIRF-Fe<sub>3</sub>O<sub>4</sub>) NPs, followed by coating the lipids consisting of tumoral hepatocytes-targeting polymer (Gal-P<sub>123</sub>). This magnetic NP (GPC@NIRF-Fe<sub>3</sub>O<sub>4</sub>) with superparamagnetic behavior showed high stability and safety in physiological conditions. In addition, GPC@NIRF-Fe<sub>3</sub>O<sub>4</sub> achieved more specific uptake of human liver cancer cells than free Fe<sub>3</sub>O<sub>4</sub> NPs. Importantly, with superparamagnetic iron oxide and strong NIR absorbance, GPC@NIRF-Fe<sub>3</sub>O<sub>4</sub> NPs demonstrate prominent tumor-contrasted imaging performance both on fluorescent and T<sub>2</sub>-weighted magnetic resonance (MR) imaging modalities in a living body. The relative MR signal enhancement of GPC@NIRF-Fe<sub>3</sub>O<sub>4</sub> NPs achieved 5.4-fold improvement compared with NIR-Fe<sub>3</sub>O<sub>4</sub> NPs. Therefore, GPC@NIRF-Fe<sub>3</sub>O<sub>4</sub> NPs may be potentially used as a candidate for dual-modal imaging of tumors with information covalidated and directly compared by combining fluorescence and MR imaging.

**Keywords:** dual-imaging, magnetic resonance imaging, hepatocellular carcinoma, tumor-targeting

## Introduction

Hepatocellular carcinoma (HCC) is the third highest cause of mortality among all malignant tumors in the world.<sup>1-3</sup> Accurate diagnosis of HCC is crucial for optimizing treatment outcomes.<sup>4</sup> Diagnostic imaging technology, including ultrasound (US), computed tomography (CT), and positron emission computed tomography (PET), has become an active area of research and has been playing a key role in HCC diagnosis.<sup>5-8</sup> Despite the diversity of bio-imaging techniques, several technical problems have yet to be solved, such as weak penetrability, low sensitivity, and insufficient spatial or temporal resolution, which hinder accurate diagnosis.<sup>9,10</sup>

Magnetic resonance imaging (MRI), with the advantages of noninvasive, multi-parametric imaging and deep soft-tissue penetration, has become a powerful technique in cancer diagnosis.<sup>11-13</sup> Superparamagnetic iron oxide nanoparticles (NPs), a kind of powerful T<sub>2</sub> contrast agent, are commonly used as magnetic vectors for MRI. Compared with gadolinium-based MRI contrast agents, including Magnevist® (Gd-DTPA; Bayer Schering Pharma, Berlin, Germany) and Multihance® (Gd-BOPTA; Bracco Diagnostics Inc., Princeton, NJ, USA),<sup>14,15</sup> superparamagnetic iron oxide NPs have been intensively investigated as promising MRI probes because of their biocompatibility and safety profiles as well as suitable magnetic properties.<sup>16-18</sup> However, limitations such as low sensitivity have hindered the further application of MRI as the sole methodology in the diagnosis

Correspondence: Juan Li  
Department of Pharmaceutics,  
China Pharmaceutical University,  
24 Tongjiaxiang, Nanjing 210009,  
People's Republic of China  
Tel +86 25 8327 1287  
Fax +86 25 8327 1766  
Email lijuanpcu@163.com

Xinxin Zhang  
Shanghai Institute of Materia Medica,  
Chinese Academy of Sciences,  
501 Haik Road, Shanghai 201203,  
People's Republic of China  
Tel +86 21 2023 1000 ext 1424  
Fax +86 21 2023 1000 ext 1425  
Email xinxinzhang@simm.ac.cn

of HCC.<sup>19–21</sup> To overcome the shortcomings, multimodal imaging techniques combining complementary advantages of different imaging modalities have attracted significant attention. For example, CT/MR imaging is obtained by multimodal contrast agents based on Au and Fe<sub>3</sub>O<sub>4</sub> NPs to get more information of tumor localization,<sup>22–24</sup> while Au shell coated on the surface of Fe<sub>3</sub>O<sub>4</sub> NPs may also result in the reduction of MRI contrast signal. Moreover, PET/MRI has been used clinically worldwide because PET is highly concentration-sensitive while supplying low resolution and MRI provides anatomic information in submillimeter range with high resolution.<sup>25,26</sup> Nevertheless, there are drawbacks; for instance, PET-MRI systems can suffer from unwanted interference between PET radiofrequencies and MRI magnetic fields.

Lately, along with the development of versatile fluorescent probes, especially near-infrared fluorescent probes, fluorescence imaging (FI) is becoming a promising tool to noninvasively resolve three-dimensional spatial distribution of fluorescent probes associated with molecular and cellular function.<sup>27</sup> Compared with other modalities, FI has several advantages, such as high sensitivity and specificity, operational simplicity, safety, and cost effectiveness,<sup>28,29</sup> though limited depth perception. Thus, the combination of FI and MRI into a single nanostructure can offer robust imaging capabilities with the prospect of improved detection accuracy in clinical diagnosis.<sup>29–31</sup> To date, there is no commercial probe available in the market with MRI/FI dual-modal capabilities. In the present study, a multifunctional nanoplateform consist of galactosyl conjugated P<sub>123</sub> (Gal-P<sub>123</sub>)-modified IR783-Fe<sub>3</sub>O<sub>4</sub> (GPC@IR783-Fe<sub>3</sub>O<sub>4</sub>) NPs was designed for dual-modal fluorescence and MR imaging of tumors. Fe<sub>3</sub>O<sub>4</sub> NPs were first labeled with IR-783 and then encapsulated in a lipid shell modified with hepatocellular carcinoma-targeting polymer (Figure 1). Gal-P<sub>123</sub> was an HCC targeting material that was synthesized in our previous study.<sup>32,33</sup> We

hypothesize that Gal-P<sub>123</sub> conjugated with fluorescence–MRI nanoparticle systems may enhance the resolution of targeting sites and supply reliable covalidation diagnosis of HCC. The formed GPC@IR783-Fe<sub>3</sub>O<sub>4</sub> NPs were characterized, and then their cytocompatibility and in vivo biocompatibility were evaluated. To demonstrate the diagnostic potential of these NPs, specific cellular uptake was examined by flow cytometry and confocal laser scanning microscopy (CLSM), and in addition, dual-modal fluorescence–MR imaging of tumor was evaluated in Huh-7 tumor-bearing mice.

## Materials and methods

### Materials

Fe<sub>3</sub>O<sub>4</sub> NPs were supplied by Shanghai Jiao Tong University (Shanghai, People's Republic of China). Gal-P<sub>123</sub> was obtained in our laboratory. Lipoid phosphatidylcholine (PC) was supplied by Lipoid GmbH (Ludwigshafen, Germany). 3-(4,5-Dimethylthiazol-2-yl)-2,5-diphenyltetrazolium bromide (MTT) was from Sigma-Aldrich (St Louis, MO, USA). All chemicals were reagent grade and used without further purification or modification.

SK-hep-1 cells were obtained from Shanghai Cell Bank, Chinese Academy of Sciences (CAS, Shanghai, People's Republic of China), and maintained in RPMI 1640 supplemented with 10% FBS, and 1% penicillin/streptomycin (Sigma-Aldrich). LO2 cells were provided by Shanghai Cell Bank, CAS, and grown in DMEM supplemented with 10% FBS (Thermo Fisher Scientific, Waltham, MA, USA) and other supplements mentioned above. All cells were kept at 37°C in a humidified and 5% CO<sub>2</sub> incubator.

### Animals and tumor xenograft models

BALB/c nude mice (18–22 g, ♂) were provided by Shanghai Laboratory Animal Center, CAS. These animals were maintained under the animal care facility for acclimatization

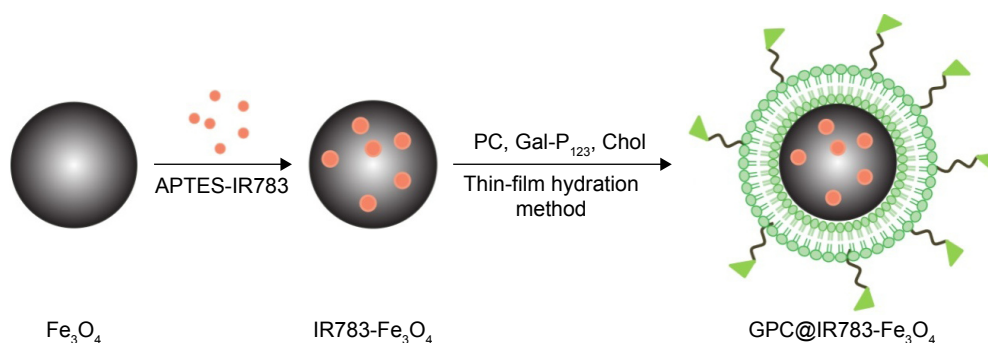


**Figure 1** Schematic illustration of the construction of GPC@IR783-Fe<sub>3</sub>O<sub>4</sub> nanoparticles (NPs).

**Abbreviations:** Gal-P<sub>123</sub>, galactosyl conjugated pluronic P<sub>123</sub>; Chol, cholesterol; APTES, aminopropyltriethoxysilane; PC, phosphatidylcholine; GPC, galactosyl conjugated pluronic P<sub>123</sub>/phosphatidylcholine.

at least 5 days prior to the experiment. Animal experiments were executed according to the protocol approved by the Institutional Animal Care and Use Committee (IACUC) of Shanghai Institute of Materia Medica, CAS. To induce solid tumor, 1 mL of hepatic carcinoma cells (Huh-7,  $1 \times 10^8$  cells in 1 mL PBS) were inoculated subcutaneously in the right armpit region of the animals.

## Preparation of multifunctional $\text{Fe}_3\text{O}_4$ NPs

Prior to the preparation of multifunctional  $\text{Fe}_3\text{O}_4$  NPs, IR-783 (or Rhodamine isothiocyanate [RITC]) was labeled to  $\text{Fe}_3\text{O}_4$  NPs. First, RITC or IR-783 was covalently bound with 3-aminopropyltriethoxysilane in ethanol, and then 10 mg of  $\text{Fe}_3\text{O}_4$  NPs were added to form the conjugation. The reaction was carried out for 8 h, and the solution was centrifuged, washed with ethanol, and ultrasonicated three times to remove the unconjugated IR-783 (or RITC) and 3-aminopropyltriethoxysilane.<sup>34</sup> Particles were collected and stored in PBS. Then, Gal-P<sub>123</sub> modified IR783- $\text{Fe}_3\text{O}_4$  (GPC@IR783- $\text{Fe}_3\text{O}_4$ ) NPs were prepared by the thin-film dispersion method. PC, Gal-P<sub>123</sub>, and Chol (Gal-P<sub>123</sub>, 3.5 mg; PC, 5.5 mg; and Chol, 0.9 mg) were dissolved in chloroform in a round flask and evaporated to form a thin film under reduced pressure. Finally, the film was dispersed in IR-783-labeled  $\text{Fe}_3\text{O}_4$  NPs solution by gentle shaking at 37°C. This was followed by extruding four times through a 200 nm-pore polycarbonate membrane with an Avestin Emulsi Flex-C5 high pressure extruder (Ottawa, ON, Canada). PC modified IR783- $\text{Fe}_3\text{O}_4$  (PC@IR783- $\text{Fe}_3\text{O}_4$ ) NPs were formulated using the same method, except that the shell consisted of PC and Chol (PC, 9 mg; Chol, 0.9 mg). Gel-filtration chromatography was used for purification of PC@IR783- $\text{Fe}_3\text{O}_4$  and GPC@IR783- $\text{Fe}_3\text{O}_4$  from the excess of uncoated lipid.

## Characterization of $\text{Fe}_3\text{O}_4$ NPs

The mean diameter and zeta potential of NPs in water were monitored by a Malvern Zetasizer Nano ZS analyzer (Malvern Instruments Ltd., Worcestershire, UK). The morphology and nanostructure of IR783- $\text{Fe}_3\text{O}_4$ , PC@IR783- $\text{Fe}_3\text{O}_4$ , and GPC@IR783- $\text{Fe}_3\text{O}_4$  were observed via transmission electron microscopy (TEM). TEM micrographs were obtained on JEOL-2010 TEM (JEOL Ltd., Tokyo, Japan) at an accelerating voltage of 200 kV.

## Vibrating sample magnetometry (VSM) analysis

The magnetic properties of IR783- $\text{Fe}_3\text{O}_4$ , PC@IR783- $\text{Fe}_3\text{O}_4$ , and GPC@IR783- $\text{Fe}_3\text{O}_4$  NPs were studied by using a VSM

(Lake Shore Cryotronics, Westerville, OH, USA) at room temperature up to  $H = 2T$ . Saturation magnetization was obtained by extrapolating to an infinite field the experimental results obtained in the high field range, where magnetization linearly increases with  $1/H$ .

## In vitro cytotoxicity study

The cell viability of IR-783-labeled iron oxide NPs on normal cell lines (LO2) was evaluated by using the standard MTT assay. LO2 cells ( $1 \times 10^4$  cells per well) were seeded in 96-well culture plates. After being cultured for 24 h, the cells were exposed to NPs with different concentrations for 24 h, after which 20  $\mu\text{L}$  5 mg/mL MTT (Sigma) solution was added. After 4 h of incubation, the medium was removed, and the cells were mixed with 150  $\mu\text{L}$  of dimethyl sulfoxide. The absorbance of solutions was measured at a test wavelength of 490 nm by a microplate reader. Relative cell viability ( $R$ ) was calculated as follows.  $R(\%) = A_{\text{test}} / A_{\text{control}} \times 100\%$ , where  $A_{\text{test}}$  and  $A_{\text{control}}$  were the absorbance of the cells treated with the test solutions and blank culture medium (FBS free) as a negative control, respectively.

## Cellular uptake of RITC-labeled $\text{Fe}_3\text{O}_4$ NPs

Huh-7 cells ( $1 \times 10^5$  cells per well) were seeded in 24-well plates and cultured at 37°C for 24 h. The medium was replaced with fresh medium; meanwhile, RITC-labeled iron oxide NPs (100  $\mu\text{g}/\text{mL}$  Fe/well) were added in the culture medium and incubated for 2 h at 37°C. Next, the cells were washed three times with ice-cold PBS and fixed with 4% paraformaldehyde for 15 min, and then washed three times with PBS. The nuclei were stained with 4',6-diamidino-2-phenylindole for 10 min and observed by CLSM.

Flow cytometry was also used to evaluate the cellular uptake of RITC-labeled  $\text{Fe}_3\text{O}_4$  NPs (100  $\mu\text{g}/\text{mL}$  Fe/well). Huh-7 cells were seeded at  $1 \times 10^5$  cells per well for 24 h at 37°C prior to the study. The cells were then incubated in medium containing RITC-labeled NPs. After 2 h of incubation, the cells were washed with PBS three times, harvested by trypsinization, and collected in PBS to quantify fluorescent signals of RITC.

## In vivo bio-fluorescence imaging

Tumor-bearing mice were injected via the tail vein at a dose of 2 mg Fe per kg of mouse body weight. A noninvasive near-infrared optical imaging system was used to observe distribution and tumor accumulation of IR-783-labeled iron oxide NPs at 1, 3, and 6 h postinjection. Visualization was

observed at excitation of 730 nm and emission of 790 nm. Tumors as well as internal organs (heart, liver, spleen, lung, and kidney) were removed at 6 h postinjection and analyzed directly on the fluorescence imager.

## In vivo MRI imaging

To investigate the iron oxide NPs' targeting potential and the MRI sensitivity of GPC@IR783-Fe<sub>3</sub>O<sub>4</sub> in vivo, MRI was performed with a 7.0T experimental MRI instrument (BioSpec 70/20 USR; Bruker, Billerica, MA, USA) on Huh-7 tumor-bearing mice. Iron oxide NPs were injected intravenously at a dose of 2 mg Fe per kg of mouse body weight, and the coronal MRI images were scanned at pre-injection and 6 h postinjection (n=3 per group). Imaging parameters were set as follows: repetition time (TR)/echo time (TE) =2,800/34 ms, field of view =4×4 cm, and slice thickness =1 mm. The signal intensity (SI) of the tumors was determined using a region of interest within the defined tumor area and normalized to the SI of the muscle tissue. Relative signal enhancement (RSE) of tumor was calculated using the following equation:<sup>35,36</sup>

$$\text{RSE (\%)} = 1 - \frac{\text{SI}_{\text{post-tumor}} / \text{SI}_{\text{post-muscle}}}{\text{SI}_{\text{pre-tumor}} / \text{SI}_{\text{pre-muscle}}} \times 100$$

SI<sub>pre</sub> and SI<sub>post</sub> were measured at preinjection and 6 h after injection.

## Histology analysis

Two hundred microliters of normal saline containing 0.8 mg of IR-783-labeled iron oxide NPs was injected intravenously into the nude mice through the tail vein. The mice were anatomized after 15 days. The paraffin sections of the heart, liver, spleen, lung, and kidney were stained with hematoxylin and eosin (H&E) and visualized by the inverted fluorescence microscope.

## Statistical analysis

Statistical analysis of all data was performed via Student's *t*-test or one-way analysis of variance (ANOVA) and expressed as mean ± SD. *P*-values less than 0.05 were considered statistically significant.

## Results and discussion

### Characterization of Fe<sub>3</sub>O<sub>4</sub> NPs

In this study, Fe<sub>3</sub>O<sub>4</sub> was labeled with IR-783 and then encapsulated in hepatocellular carcinoma-targeting polymer. The obtained NPs are biodegradable with the combined appealing

features of Fe<sub>3</sub>O<sub>4</sub> and lipids. The average size and zeta potential of IR783-Fe<sub>3</sub>O<sub>4</sub>, PC@IR783-Fe<sub>3</sub>O<sub>4</sub>, and GPC@IR783-Fe<sub>3</sub>O<sub>4</sub> NPs were determined by dynamic light scattering (Figure 2A). The average sizes of IR783-Fe<sub>3</sub>O<sub>4</sub>, PC@IR783-Fe<sub>3</sub>O<sub>4</sub>, and GPC@IR783-Fe<sub>3</sub>O<sub>4</sub> were 70.9 nm, 81.9 nm, and 83.2 nm, respectively. PC@IR783-Fe<sub>3</sub>O<sub>4</sub> and GPC@IR783-Fe<sub>3</sub>O<sub>4</sub> exhibited similar zeta potential (−12 mV), whereas IR783-Fe<sub>3</sub>O<sub>4</sub> was −30 mV. Meanwhile, the morphology of three types of NPs was detected by TEM. TEM images showed that all of the NPs possessed a regular spherical shape. Both PC@IR783-Fe<sub>3</sub>O<sub>4</sub> and GPC@IR783-Fe<sub>3</sub>O<sub>4</sub> NPs exhibited a core-shell structure, indicating the successful coating of a lipid layer on the surface (Figure 2B). As shown in Table S1, IR783-Fe<sub>3</sub>O<sub>4</sub> NPs exhibited a much bigger size compared with PC@IR783-Fe<sub>3</sub>O<sub>4</sub> and GPC@IR783-Fe<sub>3</sub>O<sub>4</sub>, implying the lipid shell acted as a dispersant to avoid possible aggregation and enhance their dispersibility. Taken together, suitable surface modification could enhance the stability of magnetic NPs in various physiological conditions and may endow Fe<sub>3</sub>O<sub>4</sub> NPs with more promising uses in the fields of bio-imaging.

## Magnetic properties

To characterize the magnetic properties of Fe<sub>3</sub>O<sub>4</sub> NPs with different coatings, the magnetization curves of IR783-Fe<sub>3</sub>O<sub>4</sub>, PC@IR783-Fe<sub>3</sub>O<sub>4</sub>, and GPC@IR783-Fe<sub>3</sub>O<sub>4</sub> obtained by using a VSM are shown in Figure 3. All NPs showed a smooth M-H curve at ambient temperature, and the saturation magnetization values of IR783-Fe<sub>3</sub>O<sub>4</sub>, PC@IR783-Fe<sub>3</sub>O<sub>4</sub>, and GPC@IR783-Fe<sub>3</sub>O<sub>4</sub> NPs were found to be 55 emu/g, 31 emu/g, and 35 emu/g, respectively. Since the shell materials do not show any significant magnetic properties, the reduction in the saturation magnetization values could be explained by decreasing the Fe<sub>3</sub>O<sub>4</sub> mass fraction in the total mass of the modified NPs.<sup>37</sup> The obtained saturation magnetization of GPC@IR783-Fe<sub>3</sub>O<sub>4</sub> NPs was lower than that of IR783-Fe<sub>3</sub>O<sub>4</sub> NPs, but it was comparable to the previously published values of magnetite NPs.<sup>37,38</sup> Because no hysteresis or remnant magnetization was observed, the superparamagnetic behavior due to the existence of Fe<sub>3</sub>O<sub>4</sub> nanocores could provide a detectable response to external magnetic field.

## Cellular uptake of Fe<sub>3</sub>O<sub>4</sub> NPs in Huh-7 cells

To evaluate the in vitro specific cellular uptake of Gal-P<sub>123</sub>-conjugated RITC-Fe<sub>3</sub>O<sub>4</sub> NPs, cell imaging was performed using CLSM with Huh-7 cells, which have a high expression of asialoglycoprotein (ASGP) receptors. As shown in Figure 4A, Huh-7 cells treated with GPC@RITC-Fe<sub>3</sub>O<sub>4</sub> NPs displayed a strong fluorescence signal. In contrast, only a

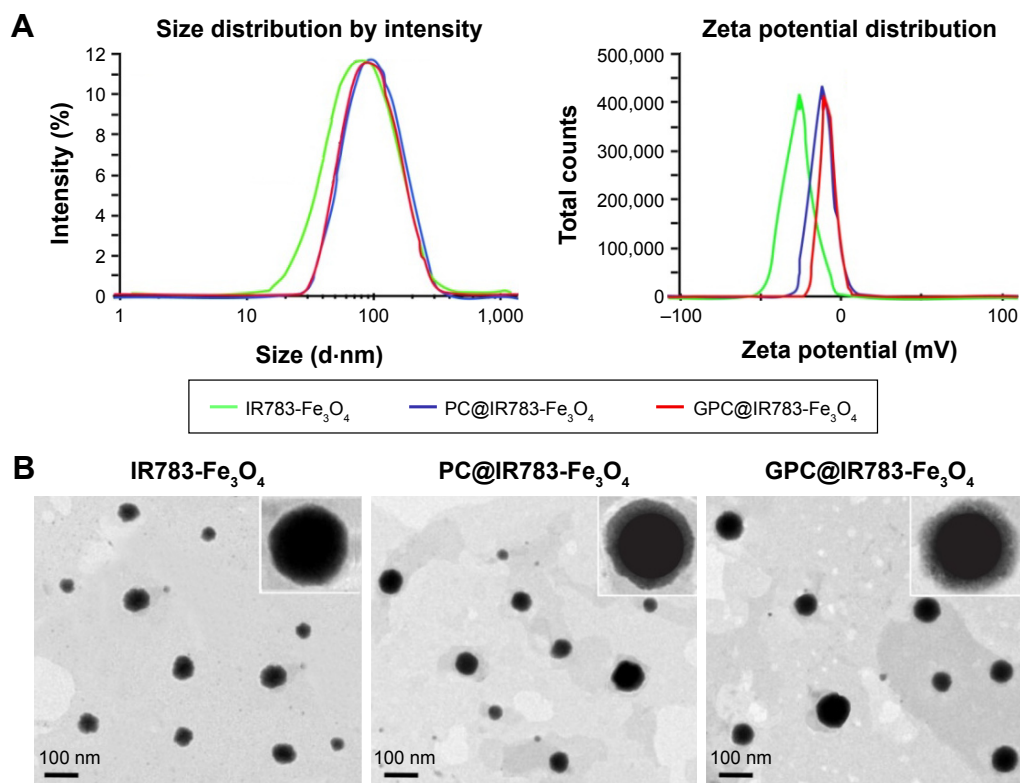


**Figure 2 (A)** Average size and zeta potential of IR783-Fe<sub>3</sub>O<sub>4</sub>, PC@IR783-Fe<sub>3</sub>O<sub>4</sub>, and GPC@IR783-Fe<sub>3</sub>O<sub>4</sub> NPs were determined by dynamic light scattering; **(B)** TEM images of IR783-Fe<sub>3</sub>O<sub>4</sub>, PC@IR783-Fe<sub>3</sub>O<sub>4</sub>, and GPC@IR783-Fe<sub>3</sub>O<sub>4</sub> NPs. The TEM images were enlarged and shown in inset images.

**Abbreviations:** PC, phosphatidylcholine; GPC, galactosyl conjugated pluronic P<sub>123</sub>/phosphatidylcholine; TEM, transmission electron microscopy; NPs, nanoparticles.

weak signal was observed in RITC-Fe<sub>3</sub>O<sub>4</sub> and PC@RITC-Fe<sub>3</sub>O<sub>4</sub>, which might be because of nonspecific adsorption.

Furthermore, the cellular uptake of RITC-labeled Fe<sub>3</sub>O<sub>4</sub> NPs by Huh-7 cells was examined over a period of 2 h by flow cytometry. Compared with RITC-Fe<sub>3</sub>O<sub>4</sub> NPs, the cellular

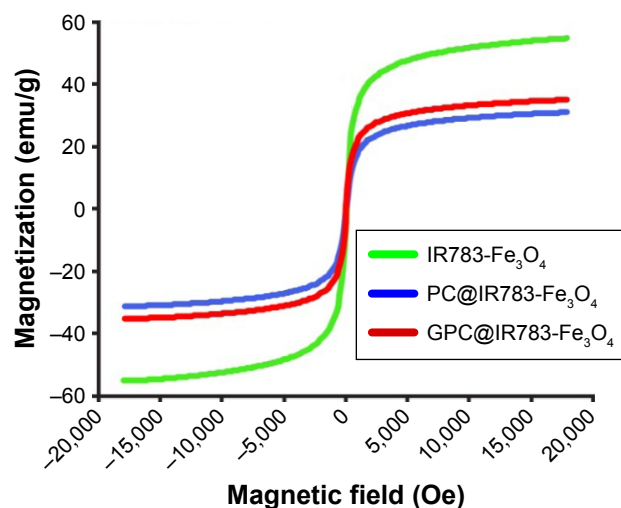


**Figure 3** VSM magnetization curves of IR783-Fe<sub>3</sub>O<sub>4</sub>, PC@IR783-Fe<sub>3</sub>O<sub>4</sub>, and GPC@IR783-Fe<sub>3</sub>O<sub>4</sub> NPs.

**Abbreviations:** PC, phosphatidylcholine; GPC, galactosyl conjugated pluronic P<sub>123</sub>/phosphatidylcholine; VSM, vibrating sample magnetometry; NPs, nanoparticles.

uptake of PC@RITC-Fe<sub>3</sub>O<sub>4</sub> and GPC@RITC-Fe<sub>3</sub>O<sub>4</sub> NPs was enhanced 2.5-fold and 4.0-fold, respectively (Figure 4B). These results implied that the lipid layer might play an important role in increasing the affinity of lipid-coated NPs to the cell membrane, and therefore promoted cellular uptake through a mechanism described as contact-facilitated delivery.<sup>39</sup> As it has been reported, ASGP receptors exhibit high affinity of Gal-modified NPs via receptor-mediated endocytosis.<sup>40</sup> Results from the flow cytometry assay were consistent with those of the CLSM imaging assay (Figure S1), confirming that Gal-P<sub>123</sub>-conjugated Fe<sub>3</sub>O<sub>4</sub> NPs displayed excellent specific uptake by Huh-7 cells.

### In vivo bio-fluorescence imaging and tumor targeting

The real-time biodistribution and tumor-targeting efficiency of IR783-Fe<sub>3</sub>O<sub>4</sub>, PC@IR783-Fe<sub>3</sub>O<sub>4</sub>, and GPC@IR783-Fe<sub>3</sub>O<sub>4</sub> administered intravenously into Huh-7 tumor-bearing nude mice were then visualized by a noninvasive near-infrared optical imaging technique at 1 h, 3 h, and 6 h postinjection. After intravenous administration of IR783-Fe<sub>3</sub>O<sub>4</sub> NPs, a strong NIRF signal was detected in the liver within 3 h postinjection, indicating rapid distribution and clearance

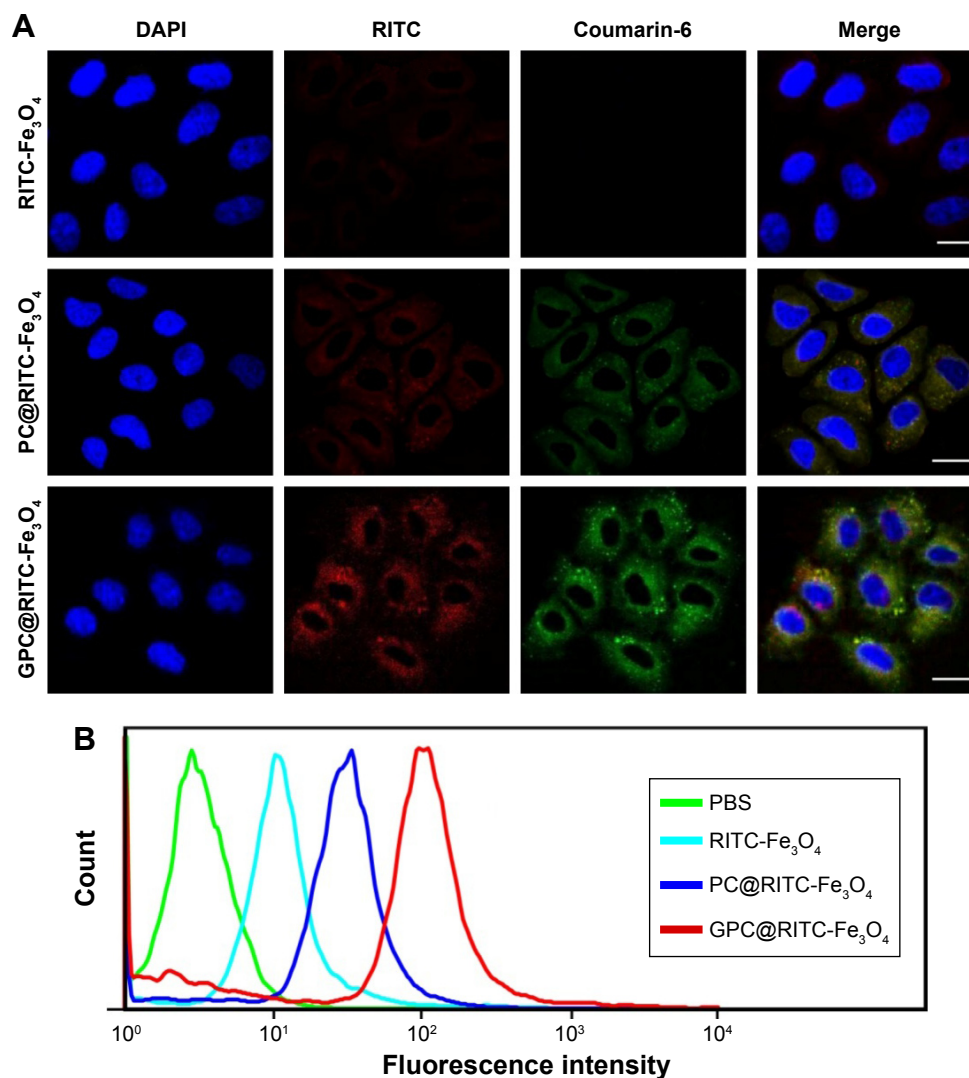


**Figure 4 (A)** CLSM images of Huh-7 with RITC-labeled Fe<sub>3</sub>O<sub>4</sub> NPs (red: RITC-Fe<sub>3</sub>O<sub>4</sub>; green: Coumarin-6 labeled with lipid; blue: nuclei) Bar: 30 μm. **(B)** Flow cytometric analysis of RITC-Fe<sub>3</sub>O<sub>4</sub>, PC@RITC-Fe<sub>3</sub>O<sub>4</sub>, and GPC@RITC-Fe<sub>3</sub>O<sub>4</sub> NPs uptake by Huh-7 cells.

**Abbreviations:** PBS, phosphate buffer saline; RITC, rhodamine isothiocyanate; PC, phosphatidylcholine; GPC, galactosyl conjugated pluronic P<sub>123</sub>/phosphatidylcholine; CLSM, confocal laser scanning microscopy; NPs, nanoparticles.

of some NPs through hepatobiliary excretion. However, GPC@IR783-Fe<sub>3</sub>O<sub>4</sub> exhibited stronger fluorescence intensity in tumor regions in quite a short time compared with other normal organs (Figure 5A). As time increased, GPC@IR783-Fe<sub>3</sub>O<sub>4</sub> showed the highest uptake in tumor; 1.7-fold higher than PC@IR783-Fe<sub>3</sub>O<sub>4</sub> and 6.1-fold higher than IR783-Fe<sub>3</sub>O<sub>4</sub>. By comparison, the signal of PC@IR783-Fe<sub>3</sub>O<sub>4</sub> showed no significant difference between tumor and normal liver tissues within 6 h postinjection (Figures S2 and 5B). The powerful tumor-targeting ability of GPC@IR783-Fe<sub>3</sub>O<sub>4</sub> could be attributed to the specific affinity of Gal-P<sub>123</sub> with ASGPR overexpressed by hepatocellular carcinoma cells. As reported previously, ASGPR is an integral membrane protein specifically expressed in hepatocytes and overexpressed in

tumor hepatocytes. Especially in tumoral hepatocytes, this overexpressed receptor loses its polarized distribution and specifically binds terminal residues of galactose, allowing the Gal-modified polymer to target to these cells.<sup>40,41</sup>

### In vivo MRI imaging application

The distribution of GPC@IR783-Fe<sub>3</sub>O<sub>4</sub> in mouse tumor tissues was also assessed by T<sub>2</sub>-weighted MR imaging. Sequential coronal images of 1 mm thickness were obtained before injection and 6 h after injection of three types of Fe<sub>3</sub>O<sub>4</sub> NPs. Figure 6A illustrates that all NPs caused contrast enhancement in the tumor sites after intravenous administration. Moreover, the injection of GPC@IR783-Fe<sub>3</sub>O<sub>4</sub> resulted in higher MR contrast in the tumor sites

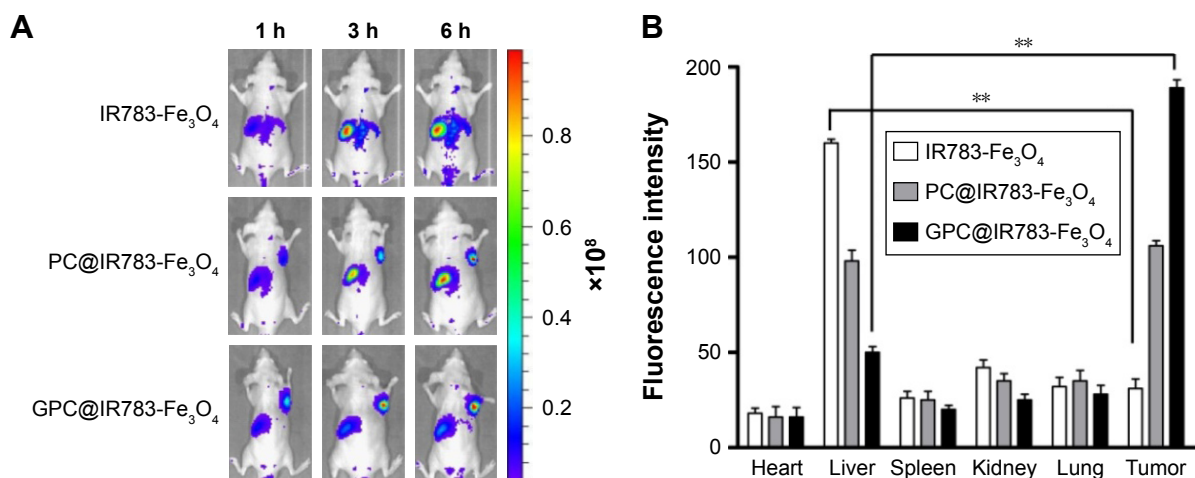


**Figure 5 (A)** In vivo bio-fluorescence imaging and tumor targeting of optical imaging technique at 1 h, 3 h, and 6 h postinjection. **(B)** Biodistribution of IR783-labeled Fe<sub>3</sub>O<sub>4</sub> NPs in major organs excised from mice at 6 h postinjection (ANOVA, \*\* $P < 0.01$  vs IR783-Fe<sub>3</sub>O<sub>4</sub>).

**Abbreviations:** PC, phosphatidylcholine; GPC, galactosyl conjugated pluronic P<sub>123</sub>/phosphatidylcholine; ANOVA, one-way analysis of variance; NPs, nanoparticles.

than PC@IR783-Fe<sub>3</sub>O<sub>4</sub> and IR783-Fe<sub>3</sub>O<sub>4</sub>, making for easy differentiation between cancer lesions and normal tissues in the MR images. RSE of Fe<sub>3</sub>O<sub>4</sub> NPs was calculated according to the SI of the defined tumor area, and the adjacent muscle is shown in Figure 6B. The RSE values of IR783-Fe<sub>3</sub>O<sub>4</sub>, PC@IR783-Fe<sub>3</sub>O<sub>4</sub>, and GPC@IR783-Fe<sub>3</sub>O<sub>4</sub> 6 h after injection were 16.3%, 40.1%, and 88.7%, respectively. The use of GPC@IR783-Fe<sub>3</sub>O<sub>4</sub> with ultrahigh T<sub>2</sub> relaxivity as contrast agent may significantly improve the sensitivity of T<sub>2</sub> imaging, which is vital for accurate detection and early diagnosis of cancer.

### In vitro and in vivo biocompatibility of GPC@IR783-Fe<sub>3</sub>O<sub>4</sub> NPs

It is necessary to ensure the biosafety of GPC@IR783-Fe<sub>3</sub>O<sub>4</sub> NPs for their potential application in medical diagnosis and bio-imaging. We evaluated the cytotoxicity of IR783-Fe<sub>3</sub>O<sub>4</sub>, PC@IR783-Fe<sub>3</sub>O<sub>4</sub>, and GPC@IR783-Fe<sub>3</sub>O<sub>4</sub> in LO2 cells by measuring cell viability via MTT assay. Figure 7A shows that the number of viable cells cultured with IR783-Fe<sub>3</sub>O<sub>4</sub>, PC@IR783-Fe<sub>3</sub>O<sub>4</sub>, and GPC@IR783-Fe<sub>3</sub>O<sub>4</sub> was nearly the same as that of blank controls when the concentrations of Fe were 125 and 250 µg/mL. And the number of viable cells was more

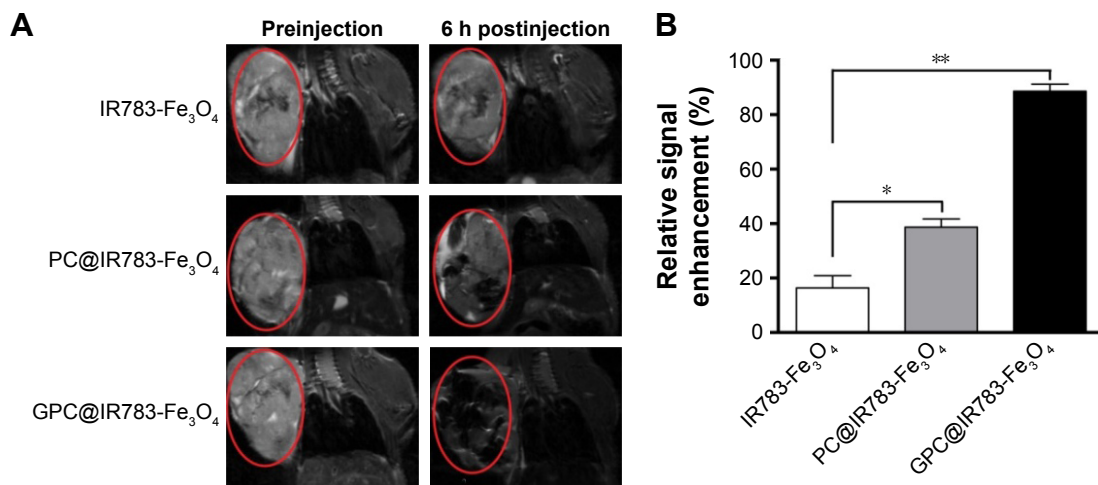


**Figure 6 (A)** In vivo coronal MRI images of BALB/c mice at 0 and 6 h after intravenous injection of IR783-Fe<sub>3</sub>O<sub>4</sub>, PC@IR783-Fe<sub>3</sub>O<sub>4</sub>, and GPC@IR783-Fe<sub>3</sub>O<sub>4</sub>. The region in the red circle was xenograft tumor. **(B)** The relative signal enhancement of the xenograft tumor in T2 MR image (ANOVA, \* $P < 0.05$  and \*\* $P < 0.01$  vs IR783-Fe<sub>3</sub>O<sub>4</sub>).

**Abbreviations:** PC, phosphatidylcholine; GPC, galactosyl conjugated pluronic P<sub>123</sub>/phosphatidylcholine; MRI, magnetic resonance imaging; ANOVA, one-way analysis of variance.

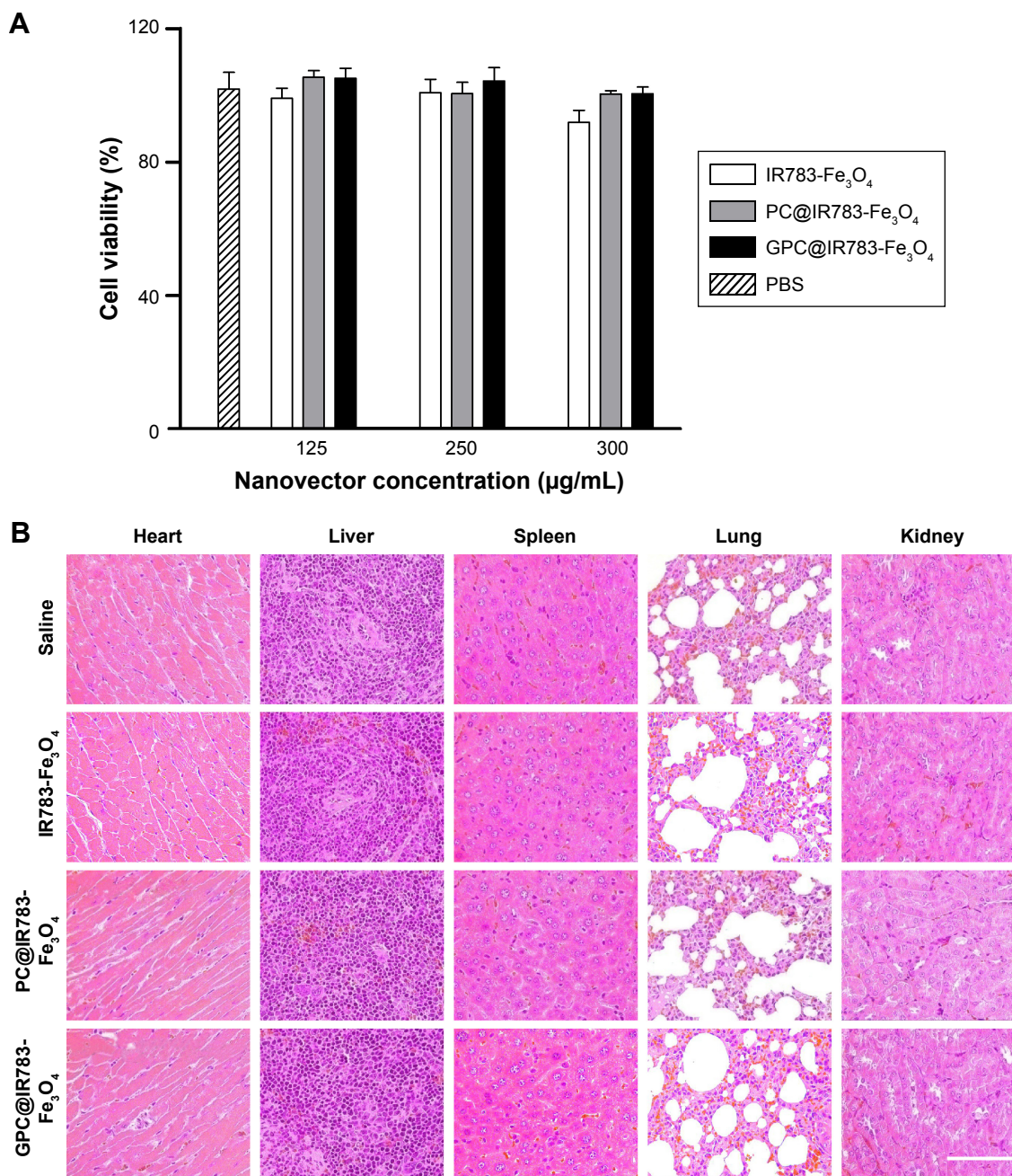


**Figure 7** Biosafety evaluation of GPC@IR783-Fe<sub>3</sub>O<sub>4</sub> NPs.

**Notes:** (A) MTT assay of LO2 cells incubated with GPC@IR783-Fe<sub>3</sub>O<sub>4</sub> NPs at various concentrations for 48 h. Cells incubated with PBS were calculated as the control. (B) Histological examination of nude mice at 15 days after injection of Fe<sub>3</sub>O<sub>4</sub> NPs. Their hearts, livers, spleens, lungs, and kidneys were stained by H&E. Untreated healthy nude mice were examined as the control. Scale bar is 100 µm.

**Abbreviations:** PC, phosphatidylcholine; GPC, galactosyl conjugated pluronic P<sub>123</sub>/phosphatidylcholine; MTT, 3-(4,5-Dimethylthiazol-2-yl)-2,5-diphenyltetrazolium bromide; PBS, phosphate buffer saline; H&E, hematoxylin and eosin; NPs, nanoparticles.

than 90% even at a high concentration of 500 µg/mL. These results demonstrated that GPC@IR783-Fe<sub>3</sub>O<sub>4</sub> NPs possess excellent cell compatibility and low cytotoxicity. To further investigate the potential toxicity *in vivo*, GPC@IR783-Fe<sub>3</sub>O<sub>4</sub> NPs were injected into the nude mice at a dose of 4 mg Fe per kg of mouse body weight. For more than 15 days, these nude mice didn't behave abnormally compared with healthy nude

mice without administration. Histological sections of their five major organs were stained with H&E. No appreciable inflammatory response, cell degeneration, necrosis, or embolism was detected between the treated organs and the normal organs, proving that GPC@IR783-Fe<sub>3</sub>O<sub>4</sub> caused no harm to the mice (Figure 7B). These results effectively provide evidence that GPC@IR783-Fe<sub>3</sub>O<sub>4</sub> should be safe for biomedical imaging.

The formed GPC@IR783-Fe<sub>3</sub>O<sub>4</sub> NPs, with the combined appealing features of Fe<sub>3</sub>O<sub>4</sub> and lipids, are biodegradable and do not seem to exert any appreciable in vivo toxicity. This can be confirmed by monitoring the physiological status of mice after intravenous treatment of NPs for at least 15 days. It should be mentioned that Gal-P<sub>123</sub> modification of the particles rendered the NPs a slightly negative surface potential and good stability in physiological conditions. Furthermore, GPC@IR783-Fe<sub>3</sub>O<sub>4</sub> showed specific affinity to ASGPR-overexpressing cancer cells in vitro and the xenografted tumor model in vivo, resulting in good tumor-targeting bio-fluorescence and MR imaging. Meanwhile, GPC@IR783-Fe<sub>3</sub>O<sub>4</sub> escaped the uptake of the reticuloendothelial system, which may avoid the unspecific distribution. With the higher and noncompromised MR imaging sensitivity, the designed NPs should be able to be used for sensitive fluorescence and MR imaging.

## Conclusion

Hepatocellular carcinoma cell-targeting fluorescence/MR dual-modality imaging NPs were successfully prepared through a convenient process. Synergistic interaction of the coated Gal-P<sub>123</sub> surface and embedded IR783-Fe<sub>3</sub>O<sub>4</sub> is vital for GPC@IR783-Fe<sub>3</sub>O<sub>4</sub> to achieve good fluorescence/MR performance as well as outstanding biocompatibility. We demonstrated that large payloads of cargo (contrast agents) were delivered to xenograft tumor by targeting ASGPR overexpressed tumoral hepatocytes in vivo. These studies suggest that GPC@IR783-Fe<sub>3</sub>O<sub>4</sub> NPs have considerable potential for further development as efficient dual-modality contrast agents for practical biomedical application.

## Acknowledgments

We are grateful for the financial support obtained from the National Natural Science Foundation of China (81571796), the Youth Innovation Promotion Association (2015229), and the SA-SIBS Scholarship Program. We also thank Prof Peng Zhang's Research Group in Shanghai Jiao Tong University for the supply of Fe<sub>3</sub>O<sub>4</sub> NPs, and Prof Jianping Zhang in Fudan University Shanghai Cancer Center for his assistance with MRI measurements and helpful discussions.

## Disclosure

The authors report no conflicts of interest in this work.

## References

1. Ferlay J, Soerjomataram I, Dikshit R, et al. Cancer incidence and mortality worldwide: sources, methods and major patterns in GLOBOCAN 2012. *Int J Cancer*. 2015;136(5):E359–E386.

2. Shiraha H, Yamamoto K, Namba M. Human hepatocyte carcinogenesis (review). *Int J Oncol*. 2013;42(4):1133–1138.
3. Torre LA, Bray F, Siegel RL, Ferlay J, Lortet-Tieulent J, Jemal A. Global cancer statistics, 2012. *CA Cancer J Clin*. 2015;65(2):87–108.
4. Waghray A, Murali AR, Menon KN. Hepatocellular carcinoma: from diagnosis to treatment. *World J Hepatol*. 2015;7(8):1020–1029.
5. Dong Y, Wang WP, Mao F, Ji ZB, Huang BJ. Application of imaging fusion combining contrast-enhanced ultrasound and magnetic resonance imaging in detection of hepatic cellular carcinomas undetectable by conventional ultrasound. *J Gastroenterol Hepatol*. 2016;31(4):822–828.
6. Kunishi Y, Numata K, Morimoto M, et al. Efficacy of fusion imaging combining sonography and hepatobiliary phase MRI with Gd-EOB-DTPA to detect small hepatocellular carcinoma. *AJR Am J Roentgenol*. 2012;198(1):106–114.
7. Wang R, Luo Y, Yang S, et al. Hyaluronic acid-modified manganese-chelated dendrimer-entrapped gold nanoparticles for the targeted CT/MR dual-mode imaging of hepatocellular carcinoma. *Sci Rep*. 2016; 6:33844.
8. Ronot M, Clift AK, Vilgrain V, Frilling A. Functional imaging in liver tumours. *J Hepatol*. 2016;65(5):1017–1030.
9. Wang J, Zhao H, Zhou Z, et al. MR/SPECT imaging guided photothermal therapy of tumor-targeting Fe@Fe<sub>3</sub>O<sub>4</sub> nanoparticles in vivo with low mononuclear phagocyte uptake. *ACS Appl Mat Interfaces*. 2016; 8(31):19872–19882.
10. Wei Z, Wu Y, Zhao Y, et al. Multifunctional nanoprobe for cancer cell targeting and simultaneous fluorescence/magnetic resonance imaging. *Anal Chim Acta*. 2016;938:156–164.
11. Situ JQ, Wang XJ, Zhu XL, et al. Multifunctional SPIO/DOX-loaded A54 homing peptide functionalized dextran-g-PLGA micelles for tumor therapy and MR imaging. *Sci Rep*. 2016;6:35910.
12. Shanavas A, Sasidharan S, Bahadur D, Srivastava R. Magnetic core-shell hybrid nanoparticles for receptor targeted anti-cancer therapy and magnetic resonance imaging. *J Colloid Interface Sci*. 2017;486:112–120.
13. Park JO, Stephen Z, Sun C, et al. Glypican-3 targeting of liver cancer cells using multifunctional nanoparticles. *Mol Imaging*. 2011; 10(1):69–77.
14. Shen Z, Wu A, Chen X. Iron oxide nanoparticle based contrast agents for magnetic resonance imaging. *Mol Pharm*. Epub 2016.
15. Lu ZR, Mohs AM, Zong Y, Feng Y. Polydisulfide Gd(III) chelates as biodegradable macromolecular magnetic resonance imaging contrast agents. *Int J Nanomedicine*. 2006;1(1):31–40.
16. Yuan Y, Ding Z, Qian J, et al. Casp3/7-Instructed Intracellular aggregation of Fe<sub>3</sub>O<sub>4</sub> nanoparticles enhances T2 MR imaging of tumor apoptosis. *Nano Lett*. 2016;16(4):2686–2691.
17. Toy R, Bauer L, Hoimes C, Ghaghada KB, Karathanasis E. Targeted nanotechnology for cancer imaging. *Adv Drug Deliv Rev*. 2014;76:79–97.
18. De M, Chou SS, Joshi HM, Dravid VP. Hybrid magnetic nanostructures (MNS) for magnetic resonance imaging applications. *Adv Drug Deliv Rev*. 2011;63(14–15):1282–1299.
19. Ma Y, Tong S, Bao G, Gao C, Dai Z. Indocyanine green loaded SPIO nanoparticles with phospholipid-PEG coating for dual-modal imaging and photothermal therapy. *Biomaterials*. 2013;34(31):7706–7714.
20. Tang Y, Zhang C, Wang J, et al. MRI/SPECT/Fluorescent tri-modal probe for evaluating the homing and therapeutic efficacy of transplanted mesenchymal stem cells in a rat ischemic stroke model. *Adv Funct Mater*. 2015;25(7):1024–1034.
21. Wei KC, Lin FW, Huang CY, et al. 1,3-Bis(2-chloroethyl)-1-nitrosourea-loaded bovine serum albumin nanoparticles with dual magnetic resonance-fluorescence imaging for tracking of chemotherapeutic agents. *Int J Nanomedicine*. 2016;11:4065–4075.
22. Wang G, Gao W, Zhang X, Mei X. Au nanocage functionalized with ultra-small Fe<sub>3</sub>O<sub>4</sub> nanoparticles for targeting T1-T2 Dual MRI and CT imaging of tumor. *Sci Rep*. 2016;6:28258.

23. Zhao HY, Liu S, He J, et al. Synthesis and application of strawberry-like Fe<sub>3</sub>O<sub>4</sub>-Au nanoparticles as CT-MR dual-modality contrast agents in accurate detection of the progressive liver disease. *Biomaterials*. 2015; 51:194–207.
24. Li J, Hu Y, Yang J, et al. Hyaluronic acid-modified Fe<sub>3</sub>O<sub>4</sub>@Au core/shell nanostars for multimodal imaging and photothermal therapy of tumors. *Biomaterials*. 2015;38:10–21.
25. Lee DH, Lee JM. Whole-body PET/MRI for colorectal cancer staging: Is it the way forward? *J Magn Reson Imaging*. 2017;45(1):25–35.
26. Goh V, Prezzi D, Mallia A, et al. Positron emission tomography/magnetic resonance imaging of gastrointestinal cancers. *Semin Ultrasound CT MR*. 2016;37(4):352–357.
27. He X, Gao J, Gambhir SS, Cheng Z. Near-infrared fluorescent nanoprobe for cancer molecular imaging: status and challenges. *Trends Mol Med*. 2010;16(12):574–583.
28. Kovar JL, Simpson MA, Schutz-Geschwender A, Olive DM. A systematic approach to the development of fluorescent contrast agents for optical imaging of mouse cancer models. *Anal Biochem*. 2007; 367(1):1–12.
29. Zhou Z, Chen H, Lipowska M, et al. A dual-modal magnetic nanoparticle probe for preoperative and intraoperative mapping of sentinel lymph nodes by magnetic resonance and near infrared fluorescence imaging. *J Biomat Appl*. 2013;28(1):100–111.
30. Wang Y, Chen J, Yang B, et al. In vivo MR and fluorescence dual-modality imaging of atherosclerosis characteristics in mice using Profilin-1 targeted magnetic nanoparticles. *Theranostics*. 2016;6(2): 272–286.
31. Zeng L, Luo L, Pan Y, Luo S, Lu G, Wu A. In vivo targeted magnetic resonance imaging and visualized photodynamic therapy in deep-tissue cancers using folic acid-functionalized superparamagnetic-upconversion nanocomposites. *Nanoscale*. 2015;7(19):8946–8954.
32. Xue WJ, Feng Y, Wang F, et al. Asialoglycoprotein receptor-magnetic dual targeting nanoparticles for delivery of RASSF1A to hepatocellular carcinoma. *Sci Rep*. 2016;6:22149.
33. Zhang X, Guo S, Fan R, et al. Dual-functional liposome for tumor targeting and overcoming multidrug resistance in hepatocellular carcinoma cells. *Biomaterials*. 2012;33(29):7103–7114.
34. Chen Y, Wang Q, Wang T. Facile large-scale synthesis of brain-like mesoporous silica nanocomposites via a selective etching process. *Nanoscale*. 2015;7(39):16442–16450.
35. Jiang L, Zhou Q, Mu K, et al. pH/temperature sensitive magnetic nanogels conjugated with Cy5.5-labeled lactoferrin for MR and fluorescence imaging of glioma in rats. *Biomaterials*. 2013;34(30):7418–7428.
36. Luo B, Wang S, Rao R, et al. Conjugation magnetic PAEEP-PLLA nanoparticles with lactoferrin as a specific targeting MRI contrast agent for detection of brain glioma in rats. *Nanoscale Res Lett*. 2016; 11(1):227.
37. Semkina A, Abakumov M, Grinenko N, et al. Core-shell-corona doxorubicin-loaded superparamagnetic Fe<sub>3</sub>O<sub>4</sub> nanoparticles for cancer theranostics. *Colloids Surf B Biointerfaces*. 2015;136:1073–1080.
38. Zhang W, Li X, Zou R, et al. Multifunctional glucose biosensors from Fe<sub>3</sub>O<sub>4</sub> nanoparticles modified chitosan/graphene nanocomposites. *Sci Rep*. 2015;5:11129.
39. Liu J, Stace-Naughton A, Jiang X, Brinker CJ. Porous nanoparticle supported lipid bilayers (protocells) as delivery vehicles. *J Am Chem Soc*. 2009;131(4):1354–1355.
40. Khorev O, Stokmaier D, Schwardt O, Cutting B, Ernst B. Trivalent, Gal/GalNAc-containing ligands designed for the asialoglycoprotein receptor. *Bioorg Med Chem*. 2008;16(9):5216–5231.
41. Trere D, Fiume L, De Giorgi LB, Di Stefano G, Migaldi M, Derenzini M. The asialoglycoprotein receptor in human hepatocellular carcinomas: its expression on proliferating cells. *Br J Cancer*. 1999;81(3): 404–408.

## Supplementary materials

### Cellular uptake of GPC@RITC-Fe<sub>3</sub>O<sub>4</sub> in different cells

Huh-7 cells ( $1 \times 10^5$  cells per well) and LO2 cells were seeded in 24-well plates and cultured at 37°C for 24 h. The medium was replaced with fresh medium; meanwhile, GPC@RITC-Fe<sub>3</sub>O<sub>4</sub> (100 µg/mL Fe/well) was added in the culture medium and incubated for 2 h at 37°C. Next, the cells were

washed three times with ice-cold PBS and fixed with 4% paraformaldehyde for 15 min, followed by washing with PBS three times. The nuclei were stained with 4',6-diamidino-2-phenylindole for 10 min and observed by CLSM.

Flow cytometry was also used to evaluate the cellular uptake of GPC@RITC-Fe<sub>3</sub>O<sub>4</sub> (100 µg/mL Fe/well) in the aforementioned two cell lines. Huh-7 cells and LO2 cells were seeded at  $1 \times 10^5$  cells per well for 24 h at 37°C prior to the study. Cells were then incubated in medium containing

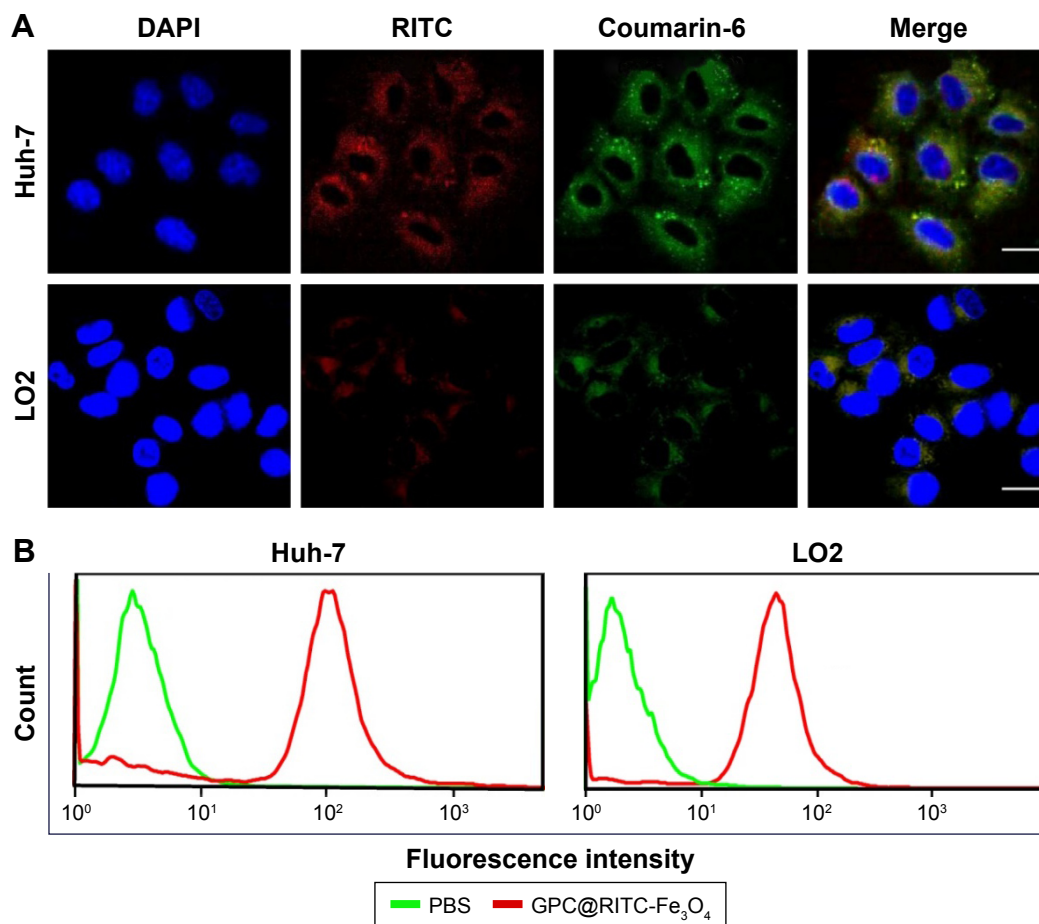


**Figure S1** (A) CLSM images of GPC@RITC-Fe<sub>3</sub>O<sub>4</sub> NPs incubated with Huh-7 cells and LO2 cells (red: RITC-Fe<sub>3</sub>O<sub>4</sub>; green: Coumarin-6 labeled in lipid; blue: nuclei) Bar: 30 µm. (B) Flow cytometric analysis of GPC@RITC-Fe<sub>3</sub>O<sub>4</sub> NPs uptake by Huh-7 cells and LO2 cells.

**Abbreviations:** RITC, rhodamine isothiocyanate; GPC, galactosyl conjugated pluronic P<sub>123</sub>/phosphatidylcholine; CLSM, confocal laser scanning microscopy; NPs, nanoparticles; PBS, phosphate-buffered saline.

**Table S1** Average size of three types of Fe<sub>3</sub>O<sub>4</sub> NPs during storage (n=3)

Fe <sub>3</sub> O <sub>4</sub> nanoparticles/ average size (nm)	Storage time (d)			
	1	7	15	30
IR783-Fe <sub>3</sub> O <sub>4</sub>	70.92±2.76	83.19±1.82	98.13±2.55	116.21±2.59
PC@IR783-Fe <sub>3</sub> O <sub>4</sub>	81.92±1.86	81.96±2.71	81.96±1.9	82.02±2.36
GPC@IR783-Fe <sub>3</sub> O <sub>4</sub>	83.2±2.64	83.18±2.81	83.21±1.75	83.26±2.97

**Notes:** Mean ± SD; n=3.

**Abbreviations:** PC, phosphatidylcholine; GPC, galactosyl conjugated pluronic P<sub>123</sub>/phosphatidylcholine; SD, standard deviation; NPs, nanoparticles.

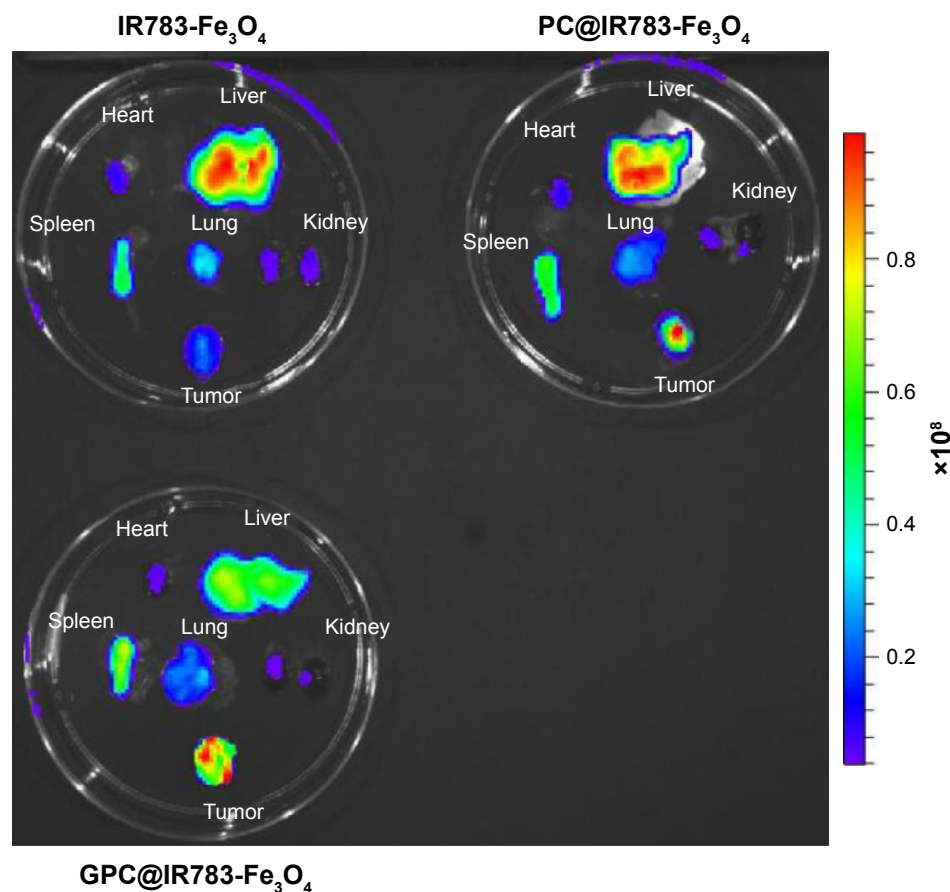


**Figure S2** Fluorescence images of organs excised at 6 h postinjection.

**Abbreviations:** PC, phosphatidylcholine; GPC, galactosyl conjugated pluronic P<sub>123</sub>/phosphatidylcholine.

GPC@RITC-Fe<sub>3</sub>O<sub>4</sub>. After 2 h of incubation, cells were washed with PBS three times, harvested by trypsinization, and collected in PBS to quantify fluorescent signals of RITC.

### In vivo bio-fluorescence imaging and tumor targeting

Tumor-bearing mice were injected via the tail vein at a dose of 2 mg Fe per kg of mouse body weight. Tumors as well

as internal organs (heart, liver, spleen, lung, and kidney) were removed at 6 h postinjection and analyzed directly on the fluorescent imager. Visualization was observed at excitation of 730 nm and emission of 790 nm. Living Image software was used to calculate the fluorescence intensity of the organs.

International Journal of Nanomedicine

**Publish your work in this journal**

The International Journal of Nanomedicine is an international, peer-reviewed journal focusing on the application of nanotechnology in diagnostics, therapeutics, and drug delivery systems throughout the biomedical field. This journal is indexed on PubMed Central, MedLine, CAS, SciSearch®, Current Contents®/Clinical Medicine,

Submit your manuscript here: <http://www.dovepress.com/international-journal-of-nanomedicine-journal>

Dovepress

Journal Citation Reports/Science Edition, EMBase, Scopus and the Elsevier Bibliographic databases. The manuscript management system is completely online and includes a very quick and fair peer-review system, which is all easy to use. Visit <http://www.dovepress.com/testimonials.php> to read real quotes from published authors.